

## Dipole pinning effect on photovoltaic characteristics of ferroelectric BiFeO<sub>3</sub> films

P. P. Biswas, Ch. Thirimal, S. Pal, and P. Murugavel

Citation: *Journal of Applied Physics* **123**, 024101 (2018);

View online: <https://doi.org/10.1063/1.5006311>

View Table of Contents: <http://aip.scitation.org/toc/jap/123/2>

Published by the *American Institute of Physics*

---

---



**Scilight**

Sharp, quick summaries **illuminating**  
the latest physics research

Sign up for **FREE!**

**AIP**  
Publishing

# Dipole pinning effect on photovoltaic characteristics of ferroelectric BiFeO<sub>3</sub> films

P. P. Biswas,<sup>1</sup> Ch. Thirimal,<sup>1,2</sup> S. Pal,<sup>1</sup> and P. Murugavel<sup>1,a)</sup>

<sup>1</sup>Department of Physics, Indian Institute of Technology Madras, Chennai 600036, India

<sup>2</sup>VNR-Vignana Jyothi Institute of Engineering and Technology, Nizampet, Hyderabad 500090, Telangana, India

(Received 24 September 2017; accepted 17 December 2017; published online 12 January 2018)

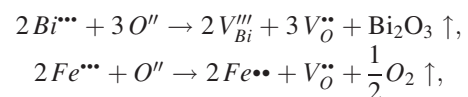
Ferroelectric bismuth ferrite is an attractive candidate for switchable devices. The effect of dipole pinning due to the oxygen vacancy layer on the switching behavior of the BiFeO<sub>3</sub> thin film fabricated by the chemical solution deposition method was studied after annealing under air, O<sub>2</sub>, and N<sub>2</sub> environment. The air annealed film showed well defined and dense grains leading to a lower leakage current and superior electrical properties compared to the other two films. The photovoltage and transient photocurrent measured under positive and negative poling elucidated the switching nature of the films. Though the air and O<sub>2</sub> annealed films showed a switchable photovoltaic response, the response was severely affected by oxygen vacancies in the N<sub>2</sub> annealed film. In addition, the open circuit voltage was found to be mostly dependent on the polarization of BiFeO<sub>3</sub> rather than the Schottky barriers at the interface. This work provides an important insight into the effect of dipole pinning caused by oxygen vacancies on the switchable photovoltaic effect of BiFeO<sub>3</sub> thin films along with the importance of stoichiometric, defect free, and phase pure samples to facilitate meaningful practical applications. *Published by AIP Publishing.* <https://doi.org/10.1063/1.5006311>

## I. INTRODUCTION

BiFeO<sub>3</sub> (BFO) is an interesting multiferroic compound due to its high temperature ferroelectric, and magnetic ordering.<sup>1</sup> The reported high polarization value ( $\sim 100 \mu\text{C}/\text{cm}^2$ ) in thin films,<sup>2</sup> attracted renewed research interest in this compound to explore its application potential in various fields.<sup>3,4</sup> Notably, the switchable polarization of BFO makes it a prospective candidate for applications in magnetoelectric random access memory (MERAM),<sup>5</sup> ferroelectric tunneling junctions (FTJs),<sup>6</sup> switchable photodiodes,<sup>7</sup> non-volatile ferroelectric based random access memory,<sup>8</sup> etc. Remarkably, BFO shows intrinsic photovoltaic (PV) response driven by the internal electric field originated from the polarization.<sup>9,10</sup> Though there are ferroelectrics like BaTiO<sub>3</sub>, LiNbO<sub>3</sub>, and Pb(Zr, Ti)O<sub>3</sub> exhibiting PV response,<sup>11–13</sup> BFO stands alone due to its superior ferroelectric properties and desirable optical bandgap (2.1–2.7 eV) for PV applications.<sup>14</sup>

Note that the photovoltaic response, in particular, its unique switchable characteristics are quite sensitive to the defects in the films. It is known that the defects in general have a disparaging effect on the ferroelectric characteristics, in particular, to domain switching. The role of defects on domain pinning is well studied for systems like Pb(Zr,Ti)O<sub>3</sub>, (Ba,Sr)TiO<sub>3</sub>, Bi<sub>4</sub>Ti<sub>3</sub>O<sub>12</sub>, and K<sub>0.5</sub>Na<sub>0.5</sub>NbO<sub>3</sub>.<sup>15–18</sup> Among various defects, oxygen vacancies and their complexing with other defects are thought to be responsible for dipole pinning. Controlling the stoichiometric composition and the resultant oxygen vacancies is always a challenging task in the BFO sample due to the volatile Bi and mixed valence state of Fe<sup>3+</sup>/Fe<sup>2+</sup>. The possible charge compensation mechanism

responsible for the formation of oxygen vacancies written in the Kroger-Vink notation is given as follows:<sup>19</sup>



where  $Fe^{\bullet\bullet\bullet}$ ,  $Bi^{\bullet\bullet\bullet}$ , and  $O''$  are iron, bismuth, and oxygen ions in the lattice, respectively.  $V_{Bi}^{\prime\prime\prime}$  and  $V_O^{\bullet\bullet}$  denote the bismuth and oxygen vacancies, whereas the prime and dot represent the negative and positive charges, respectively.

Looking at the recent flurry of research activity on the PV capability of BFO samples, it is highly indispensable to understand the role of oxygen vacancies on the PV characteristics of BFO films to realize their application potential. Though there are few reports on the effect of oxygen vacancy on the PV effect,<sup>20–22</sup> not many are focused on the effect of oxygen vacancy due to the annealing atmosphere. To address this issue, we have carried out PV studies on BFO films annealed under air and O<sub>2</sub> atmospheric conditions along with the sample annealed in the N<sub>2</sub> condition to deliberately increase the concentration of oxygen vacancies. The detailed studies on the role of oxygen vacancies and thereby the defect dipoles on the switchable characteristics of open circuit voltage ( $V_{OC}$ ) and transient photocurrent density ( $J$ ) are presented in this work.

## II. EXPERIMENTAL DETAILS

Polycrystalline BFO films of 350 nm thickness were fabricated on (111)Pt/TiO<sub>2</sub>/SiO<sub>2</sub>/Si(100) substrates using the spin coating technique. The detailed procedure is adopted from the previously reported work,<sup>23</sup> except for the annealing temperature which was done at 550 °C for 1 h. The

<sup>a)</sup>Author to whom correspondence should be addressed: muruga@iitmadras.ac.in

grown films were subjected to annealing under three different atmospheric conditions such as air, oxygen ( $O_2$ ), and nitrogen ( $N_2$ ). The annealed films were characterized for their phase and morphology by an X-ray diffractometer (Rigaku-Smart lab) and a F50 field emission scanning electron microscope (FESEM), respectively. The polarization versus voltage measurements were carried out using a Radiant ferroelectric tester (Precision premiere II USA) at 25 kHz. Semi-transparent, 18 nm thick Au dots of 200  $\mu\text{m}$  diameter were used as top electrodes [see Figs. S1 and S2 (supplementary material) for the thickness profile and optical transmission spectra of Au on the silicon and glass substrate, respectively] and the resultant Au/BFO/Pt geometry was poled with  $\pm 7\text{ V}$ . For the positive and negative poling, the voltages are applied with respect to the bottom electrode. Photovoltaic measurements were carried out by using a Keithley high resistance electrometer (6517B) under the light illumination from a Xenon arc lamp source (Newport 67005) with the spectral range from 250 nm to 2500 nm and the light power density used was 166  $\text{mW}/\text{cm}^2$ .

### III. RESULTS AND DISCUSSION

#### A. Structural and morphological analysis

The X-ray diffraction (XRD) patterns performed on the BFO samples annealed under different atmospheric conditions are shown in Fig. 1 for the  $2\theta$  range of  $20^\circ$  to  $60^\circ$ . The substrate peaks are not visible in the patterns because the XRD measurements are carried out under the glancing angle  $\omega = 5^\circ$ . The patterns reveal that the samples are polycrystalline in nature. Note that the air annealed BFO sample shows a clean XRD pattern with the peaks corresponding to its rhombohedral crystal structure. On the other hand, BFO films annealed under  $O_2$  and  $N_2$  conditions exhibit a trace amount of  $\text{Bi}_{36}\text{Fe}_2\text{O}_{57}$  secondary phase (marked by \* in the

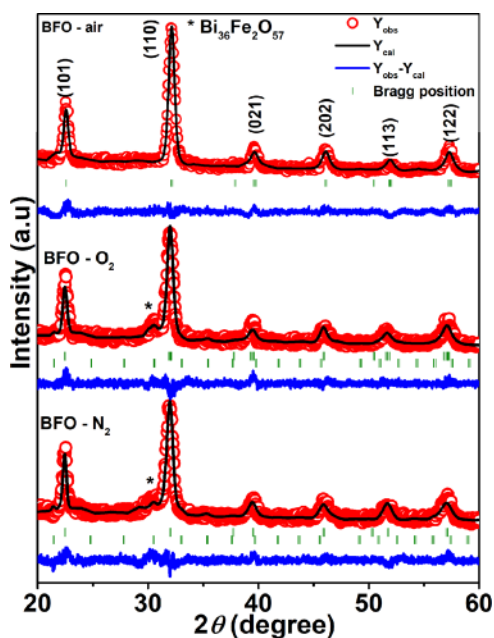


FIG. 1. X-ray diffraction patterns and Rietveld analysis for BFO annealed in the air,  $O_2$ , and  $N_2$  atmosphere.

patterns) along with the major rhombohedral BFO phase. The formation of the secondary phase reiterates the reported narrow thermodynamical conditions existing for phase pure BFO synthesis.<sup>24,25</sup>

In addition, the Rietveld refinements are performed on XRD of BFO films annealed in the air,  $O_2$ , and  $N_2$  atmosphere. While performing Rietveld refinements of BFO annealed in the  $O_2$  and  $N_2$  atmosphere, the impurity phase  $\text{Bi}_{36}\text{Fe}_2\text{O}_{57}$  is considered as the cubic phase with space group I23 along with the rhombohedral structure of BFO with space group R3c. The results of the Rietveld refinements are also shown in Fig. 1 and the extracted structural parameters are given in Table I. It is found that, there is an increase in the lattice parameter along with volume for both  $O_2$  and  $N_2$  annealed samples, and these structural changes are mostly related to the non-stoichiometry in the BFO composition due to the segregation of impurity phases.

To observe the annealing atmospheric effect on the surface morphology, FESEM studies are performed and the resultant images for air,  $O_2$ , and  $N_2$  annealed films are shown in Figs. 2(a)–2(c), respectively. The figures reveal that the films show distinct morphological differences upon annealing under various atmospheric conditions. The ambient annealed BFO displays a well defined grain-like structure with an average grain size of around 250 nm. But, when the films are annealed under  $O_2$  and  $N_2$  conditions, the grain-like structure is lost and the surface looks rough with more agglomerated particles. Note that the XRD patterns reveal only a trace amount of secondary phase which cannot be completely accountable for the observed surface nature. Possibly, the other reason could come from the oxygen nonstoichiometric and the resultant diffusion of cationic vacancies.

#### B. Leakage current and ferroelectric properties

To investigate the effect of annealing conditions on the leakage characteristics of the fabricated films, current is measured as a function dc voltage in the range of  $\pm 1.2\text{ V}$ . The respective plot between current versus applied voltage for all the films is shown in Fig. 3(a). The figure indicates that though the observed leakage currents are typically of the order reported for good ferroelectric samples ( $< 10^{-6}\text{ A}$ ), the leakage current of  $O_2$  and  $N_2$  annealed films display an order of higher magnitude value ( $10^{-9}\text{ A}$ ) in comparison to the film annealed in air ( $10^{-10}\text{ A}$ ). In general, the leakage current depends on factors like phase purity, grain size, oxygen nonstoichiometry, etc. Hence, the observed variation in leakage current behavior in the annealed samples can be correlated to both phase purity and the effect of oxygen non-stoichiometry in the films.

TABLE I. Extracted lattice parameters  $a$ ,  $b$ ,  $c$ , volume, and the fitting parameter  $\chi^2$  from the Rietveld refinement.

	$a$ (Å)	$b$ (Å)	$c$ (Å)	Volume (Å <sup>3</sup> )	$\chi^2$
BFO-air	5.5737	5.5737	13.6194	366.41	1.85
BFO- $O_2$	5.5759	5.5759	13.7569	370.42	1.27
BFO- $N_2$	5.5914	5.5914	13.6957	370.82	1.53

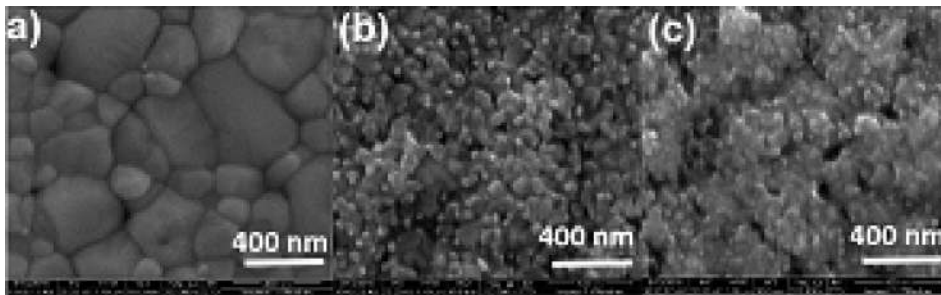


FIG. 2. Scanning electron microscopic surface images of BFO annealed in (a) air, (b)  $O_2$ , and (c)  $N_2$  atmosphere.

For the ferroelectric characteristics, polarization ( $P$ ) versus voltage ( $V$ ) measurements are carried out and the results are presented in Fig. 3. As expected from the low leakage current, all films unveil typical  $P$ - $V$  hysteresis loops. The film annealed under air exhibits a large remnant polarization ( $P_r = 14 \mu C/cm^2$ ), while the films annealed under  $O_2$  and  $N_2$  display reduction in  $P_r$  such as  $4.7 \mu C/cm^2$  and  $2.9 \mu C/cm^2$ , respectively. Note that though similar reduction in  $P_r$  is observed for both  $O_2$  and  $N_2$  annealed films, the later one displays an asymmetric  $P$ - $V$  loop where the loop is seen shifting towards right. Shifted  $P$ - $V$  loops are generally observed when there is a pinning of domain by defects present in the films.<sup>26</sup> Similar such loops are reported in  $BaTiO_3$ ,  $Pb(Zr,Ti)O_3$ , and  $(Ba,Ca)TiO_3$ , where the defects responsible for pinning are corroborated to acceptor-oxygen type vacancy dipoles.<sup>27-29</sup> Considering the shape of the  $P$ - $V$  loops, the sample looks relatively leaky, therefore positive-up-negative-down (PUND) measurement is carried out to get the actual remnant polarization without any leakage effect. The PUND measurement, as shown in Fig. S3 (supplementary material), reveals switchable polarization. The remnant polarizations for positive ( $dP/2 = 6.38 \mu C/cm^2$ ) and negative ( $-dP/2 = 6.23 \mu C/cm^2$ ) applied fields are calculated as  $dP/2 = (P^* - P^\wedge)/2$  and  $-dP/2 = (-P^* - (-P^\wedge))/2$ , respectively,

where  $P^*$  contains both remnant as well as non-remnant polarization, whereas  $P^\wedge$  contains only the non-remnant polarization.  $P_r^*$  and  $P_r^\wedge$  are equivalent polarizations of  $P^*$  and  $P^\wedge$ , respectively, measured when the applied electric field is reduced to zero in the subsequent pulse.

### C. Effect of annealing atmosphere on the switchable photovoltaic effect

To investigate the PV response of BFO films with respect to its different defect level created by the annealing conditions, current density ( $J$ ) versus voltage ( $V$ ) measurements are carried out and the schematic diagram depicting the experimental arrangement used for photovoltaic measurements is shown in Fig. 4(a). The PV curves obtained under dark and illumination conditions for air,  $O_2$ , and  $N_2$  annealed films are shown in Figs. 4(b)–4(d), respectively. Note that the BFO films did not show any PV response under unpoled conditions irrespective of the annealing conditions. As a representative example, the  $J$ - $V$  data recorded in dark and light for the air annealed sample under the unpoled condition are shown in Fig. 4(b). On the other hand, the films under study display PV characteristics only under poling conditions. Notably, the behavior of the acquired  $J$ - $V$  curves

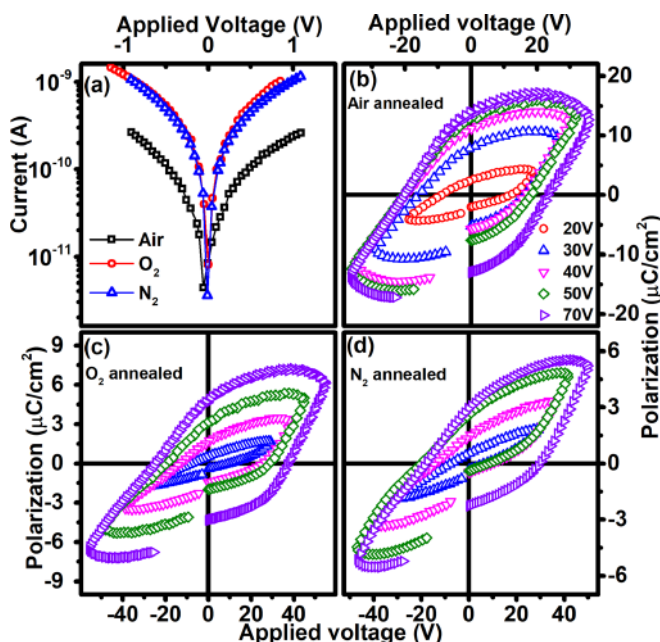


FIG. 3. (a) Leakage current versus voltage plots for BFO films annealed in different atmospheres.  $P$ - $V$  hysteresis loops for (b) air, (c)  $O_2$ , and (d)  $N_2$  annealed BFO films.

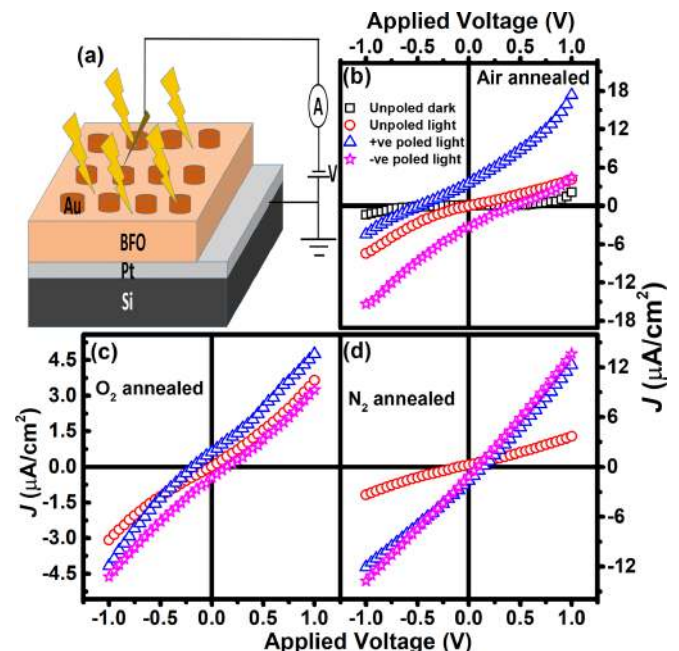


FIG. 4. (a) Schematic diagram showing the geometry used for photovoltaic measurement. The photovoltaic  $J$  versus  $V$  curves for (b) air, (c)  $O_2$ , and (d)  $N_2$  annealed BFO films for poled and unpoled states.

for all samples ruled out the significant contribution from the Schottky-type junction at the interface between the electrode and film. Hence, the observed  $J$ - $V$  curves under poled conditions strongly suggest that the PV response of BFO films could originate from the depolarization field which is responsible for the separation of photogenerated electron hole pairs.<sup>9</sup> Under negatively poled conditions,  $V_{OC}$  for air,  $O_2$ , and  $N_2$  annealed films are 0.45, 0.14, and 0.13 V, respectively. The decrease in  $V_{OC}$  for  $O_2$  and  $N_2$  annealed films could be due to reduction in the remnant polarization of these films in comparison to the air annealed film as seen from Fig. 2. On the other hand, the respective  $V_{OC}$  values for positively poled conditions are  $-0.47$ ,  $-0.2$ , and  $0.14$  V. Note that both air and  $O_2$  annealed films exhibit switchable  $V_{OC}$  between positive and negative poling conditions. However, the  $N_2$  annealed film shows positive  $V_{OC}$  irrespective of the sign of the poling voltage.

To examine the major contribution of the depolarization field in the observed PV effect,  $J$ - $V$  measurement is done under illumination by poling the BFO-air annealed sample at different poling voltages. Figure S4 (supplementary material) demonstrates that, the switchable PV is observed at all poling voltages. However, at a low poling voltage, the  $J$ - $V$  curves reveal diode like characteristics with poling direction dependent asymmetric features. The observed asymmetric features at the low poling voltage may be due to incomplete switching of dipoles along with the Schottky effect at the interface. On the other hand, the complete absence of these features at a high poling voltage ( $\pm 7$  V) without any significant Schottky diode effect strongly indicates that the major contribution to the PV could come from the depolarization field (Fig. S4, supplementary material). The poling voltage is restricted to ( $\pm 7$  V), beyond which the sample shows voltage breakdown.

To elucidate further, the short circuit current under light ON-OFF conditions in positive and negative poled BFO films is measured with respect to time under a zero bias voltage (short circuit condition). The resultant  $J$  versus time plots are shown in Figs. 5(a)–5(c) for air,  $O_2$ , and  $N_2$  annealed films, respectively. The figure illustrates that all samples display quick and stable photo-induced current under the light ON condition. As the light is turned on, the current shoots up and reaches saturation within a short time. Similarly, when the light is turned off, the current drops down from its saturated value to zero. Such sharp photo-response makes BFO an attractive candidate for photosensitive device applications. In principle, for a perfect PV system, the short circuit current at zero bias should be constant; however, the role of the pyroelectric effect cannot be completely neglected. The observed gradual initial increase in current is due to pyro-current. As expected, Figs. 5(a) and 5(b) reveal switchable transient photocurrent characteristics for air and  $O_2$  annealed films. Whereas, the  $N_2$  annealed film reveals a non-switchable transient photocurrent as evidenced from Fig. 5(c). The non-switchable PV nature of the film can have direct correlation with the dipole pinning. It is reported that one of the possible reasons for dipole pinning and non-switchable PV characteristics could originate from the oxygen vacancy layer formed at the film-substrate interface.<sup>30</sup> As a result, the vacancies at the interface pin the domains

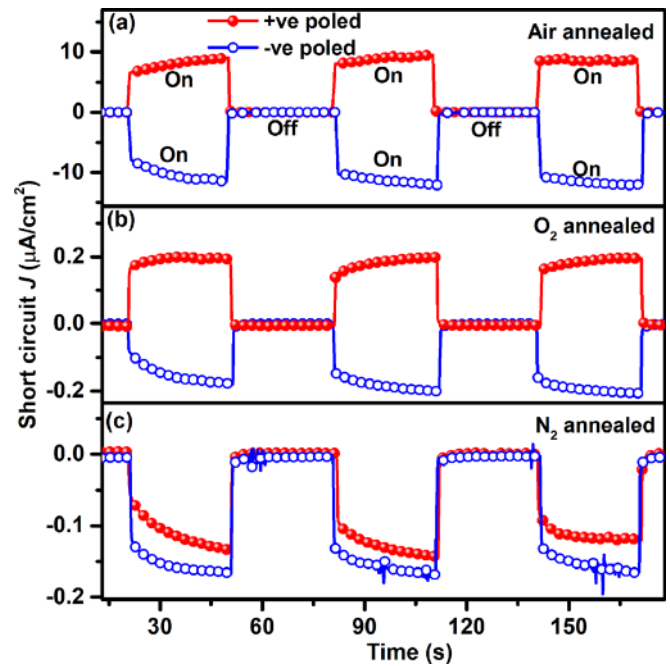


FIG. 5. Transient short circuit photocurrent measured as a function of time under the light ON and OFF state for BFO films annealed in (a) air, (b)  $O_2$ , and  $N_2$  atmosphere.

and allow to switch only in certain preferred directions. Generally, the oxide films annealed in the  $N_2$  atmosphere end up having a large number of oxygen vacancies compared to the films annealed in air and  $O_2$  conditions, thereby creating a dense oxygen vacancy layer at the bottom interface. The additional possible mechanisms responsible for oxygen vacancies in the BFO film annealed in the  $N_2$  atmosphere are given as follows:<sup>31</sup>



Here, two  $N^{3-}$  anions replace two  $O^{2-}$  anions in the sublattice with generation of an oxygen vacancy in the lattice. The oxygen vacancy layer at the BFO/Pt interface responsible for the defect dipoles and the pinning effect is the main cause for the observed shifted  $P$ - $V$  hysteresis loop along with the non-switchable character of the photovoltaic response in  $N_2$  annealed sample. Note that according to Matsuo *et al.*, the defective layer (oxygen-vacancy rich layer) formed by accumulation of  $V_O^{**}$ , generally occurs at the BFO/Pt interface during the film processing conditions (deposition, pre-heating, and annealing process).<sup>32</sup>

#### IV. CONCLUSION

To understand the effect of defect dipoles on the PV characteristics of  $BiFeO_3$  films, the PV studies were done on films annealed under air,  $O_2$ , and  $N_2$  environment. The films were crystallized in the rhombohedral phase. The ferroelectric characteristics of these films studied from the  $P$ - $V$  hysteresis measurements revealed a decrease in polarization for  $O_2$  and  $N_2$  annealed samples compared to the air annealed sample. In addition, the  $N_2$  annealed sample exhibited a shifted hysteresis loop indicating the presence of domain

pinning. The PV measurements on air and O<sub>2</sub> annealed samples displayed almost symmetric and switchable current versus voltage curves, but with a reduction in  $V_{OC}$  in the later case. However, though the N<sub>2</sub> annealed film displayed typical photovoltaic  $J$ - $V$  curves, its switchable characteristics were lost due to domain pinning. The cause of domain pinning is attributed to the formation of an oxygen vacancy layer at the electrode sample interface during the annealing process. Overall, the effect of domain pinning caused by oxygen vacancies on the PV features of the BFO thin film was clearly elucidated. These results convey the importance of improving the stoichiometric, defect free, and phase pure BFO sample to maximize its application potential especially in photovoltaic studies.

## SUPPLEMENTARY MATERIAL

See [supplementary material](#) available in the online version of the paper for further details about the thickness and transparency of the gold electrode, PUND measurement for the BFO film, and PV measurements on the BFO film performed under different poling voltages.

## ACKNOWLEDGMENTS

This work was supported by the Nanomission-DST Project No. SR/NM/NS-05/2012(G). We acknowledge Professor Ratnamala Chatterjee, IIT Delhi, for the  $P$ - $V$  measurements.

<sup>1</sup>V. G. Bhide and M. S. Multani, *Solid State Commun.* **3**, 271 (1965).

<sup>2</sup>K. Y. Yun, D. Ricinchi, T. Kanashima, and M. Okuyama, *Appl. Phys. Lett.* **89**, 192902 (2006).

<sup>3</sup>B. Noheda, D. E. Cox, G. Shirane, J. A. Gonzalo, L. E. Cross, and S. E. Park, *Appl. Phys. Lett.* **74**, 2059 (1999).

<sup>4</sup>H. Bea, M. Gajek, M. Bibes, and A. Barthelémy, *J. Phys.: Condens. Matter* **20**, 434221 (2008).

<sup>5</sup>M. Bibes and A. Barthelémy, *Nat. Mater.* **7**, 425 (2008).

<sup>6</sup>H. Yamada, V. Garcia, S. Fusil, S. Boyn, M. Marinova, A. Gloter, S. Xavier, J. Grollier, E. Jacquet, C. Carrétéro, C. Deranlot, M. Bibes, and A. Barthelémy, *ACS Nano* **7**, 5385 (2013).

<sup>7</sup>P. Nayek and G. Li, *Sci. Rep.* **5**, 10845 (2015).

<sup>8</sup>R. Guo, L. You, Y. Zhou, Z. S. Lim, X. Zou, L. Chen, R. Ramesh, and J. Wang, *Nat. Commun.* **4**, 1990 (2013).

<sup>9</sup>M. Alexe and D. Hesse, *Nat. Commun.* **2**, 256 (2011).

<sup>10</sup>T. Choi, S. Lee, Y. J. Choi, V. Kiryukhin, and S.-W. Cheong, *Science* **324**, 63 (2009).

<sup>11</sup>J. E. Spanier, V. M. Fridkin, A. M. Rappe, A. R. Akbashev, A. Polemi, Y. Qi, Z. Gu, S. M. Young, C. J. Hawley, D. Imbrenda, G. Xiao, A. L. Bennett-Jackson, and C. L. Johnson, *Nat. Photonics* **10**, 611 (2016).

<sup>12</sup>V. M. Fridkin and B. N. Popov, *Sov. Phys. Usp.* **21**, 981 (1978).

<sup>13</sup>E. Dubovik, V. Fridkin, and D. Dimos, *Integr. Ferroelectr.* **8**, 285 (1995).

<sup>14</sup>V. Železný, D. Chvostová, L. Pajasová, I. Vrejoiu, and M. Alexe, *Appl. Phys. A* **100**, 1217 (2010).

<sup>15</sup>X. B. Ren, *Nat. Mater.* **3**, 91 (2004).

<sup>16</sup>L. X. Zhang, W. Chen, and X. B. Ren, *Appl. Phys. Lett.* **85**, 5658 (2004).

<sup>17</sup>N. Zhong, P. H. Xiang, Y. Y. Zhang, X. Wu, X. D. Tang, P. X. Yang, C. G. Duan, and J. H. Chu, *J. Appl. Phys.* **118**, 104102 (2015).

<sup>18</sup>D. M. Lin, K. W. Kwok, and H. L. W. Chan, *Appl. Phys. Lett.* **90**, 232903 (2007).

<sup>19</sup>G. L. Yuan and S. W. Or, *J. Appl. Phys.* **100**, 024109 (2006).

<sup>20</sup>Y. Guo, B. Guo, W. Dong, H. Li, and H. Liu, *Nanotechnology* **24**, 275201 (2013).

<sup>21</sup>R. L. Gao, H. W. Yang, Y. S. Chen, J. R. Sun, Y. G. Zhao, and B. G. Shen, *Appl. Phys. Lett.* **104**, 031906 (2014).

<sup>22</sup>M. Yang, A. Bhatnagar, and M. Alexe, *Adv. Electron. Mater.* **1**, 1500139 (2015).

<sup>23</sup>A. Srivastava, A. Garg, and F. D. Morrison, *J. Appl. Phys.* **105**, 054103 (2009).

<sup>24</sup>K. Prashanthi, M. Gupta, Y. Y. Tsui, and T. Thundat, *Appl. Phys. A* **110**, 903 (2013).

<sup>25</sup>A. Z. Simões, C. S. Riccardi, M. L. Dos Santos, F. González Garcia, E. Longo, and J. A. Varela, *Mater. Res. Bull.* **44**, 1747 (2009).

<sup>26</sup>M. I. Morozov and D. Damjanovic, *J. Appl. Phys.* **104**, 034107 (2008).

<sup>27</sup>P. V. Lambeck and G. H. Jonker, *J. Phys. Chem. Solids* **47**, 453 (1986).

<sup>28</sup>K. Carl and K. H. Hardtl, *Ferroelectrics* **17**, 473 (1977).

<sup>29</sup>S. Yun, X. Wang, J. Shi, and D. Xu, *J. Mater. Res.* **24**, 3073 (2009).

<sup>30</sup>D. Lee, S. H. Baek, T. H. Kim, J. G. Yoon, C. M. Folkman, C. B. Eom, and T. W. Noh, *Phys. Rev. B* **84**, 125305 (2011).

<sup>31</sup>T. Bräuniger, T. Müller, A. Pampel, and H. P. Abicht, *Chem. Mater.* **17**, 4114 (2005).

<sup>32</sup>H. Matsuo, Y. Kitanaka, R. Inoue, Y. Noguchi, and M. Miyayama, *J. Appl. Phys.* **118**, 114101 (2015).